

Dynamical Windings of Random Walks and Exclusion Models.

Part I: Thermodynamic Limit

Guy Fayolle Cyril Furtlehner

Abstract

We consider a system consisting of a planar random walk on a square lattice, submitted to stochastic elementary local deformations. Both numerical and theoretical results are reported. Depending on the deformation transition rates, and specifically on a parameter η which breaks the symmetry between the left and right orientation, the winding distribution of the walk is modified, and the system can be in three different phases: folded, stretched and glassy. An explicit mapping is found, leading to consider the system as a coupling of two exclusion processes: particles of the first one move in a landscape defined by particles of the second one, and vice-versa. This can be viewed as an inhomogeneous exclusion process. For all closed or periodic initial sample paths, a convenient scaling permits to show a convergence in law (or almost surely on a modified probability space) to a continuous curve, the equation of which is given by a system of two non linear stochastic differential equations. The deterministic part of this system is explicitly analyzed via elliptic functions. In a similar way, by using a formal fluid limit approach, the dynamics of the system is shown to be equivalent to a system of two coupled Burgers' equations.

1 Introduction

Random walks are fundamental objects arising in probability. Also they are of primary importance in various fields of physics, especially with regard to polymers [1, 2] and biology. For instance, planar random walks can be used as a representation of DNA coding, since the sequence of the four different kinds of codons (A,G) for purines and (T,C) for pyrimidines can be considered as a random walk on a square lattice: as a rule, (G,C) code the upward and downward jumps, whereas (A,T) code the left and right steps [6, 8]. It seems therefore interesting to consider random geometrical objects as complex systems, and to submit them to some dynamical principles, the goal being to develop methods and tools which hopefully might be used to tackle more realistic models.

In this context we will analyze the evolution of an arbitrary sample path \mathbf{C}_N of length N , generated by a *simple* random walk in the square lattice \mathbf{Z}^2 , and subject to local transformations. This stochastic object has a rich structure, plays an

important role in probability theory and lends itself to sufficiently wide but non trivial results.

At time $t = 0$, \mathbf{C}_N is given, and we assume it has been uniformly generated. This means precisely that each successive jump (up, down, left and right) building \mathbf{C}_N is selected with the same probability $1/4$. Eventually \mathbf{C}_N can be constrained to be closed or to have fixed extremities. Once the initial configuration is defined, the system evolves according to the four local pattern transformations depicted in Figure 1.1. Only a single point of the walk can be moved at a time, with the constraint that no link be broken (i.e. the walk remains always connected).

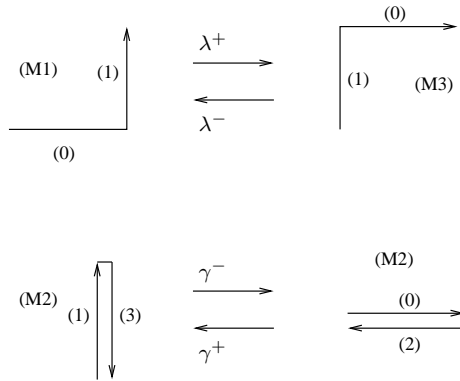


Fig. 1.1: Pattern transition rates.

Geometrically, these patterns can be expressed as

$$\begin{cases} \text{left bend } M1, \text{ right bend } M3, \\ \text{vertical or horizontal fold } M2, \\ \text{straight } (\rightarrow\rightarrow) M4, \end{cases}$$

and the following local distortions can occur:

$$\begin{cases} M1 \rightarrow M3, \text{ with rate } \lambda^+, \\ M3 \rightarrow M1, \text{ with rate } \lambda^-, \\ \text{rotation of } M2 \text{ of angle } \pm \frac{\pi}{2}, \text{ with rate } \gamma^\pm. \end{cases}$$

Hence we have defined a global Markovian continuous time evolution of the system, with exponentially distributed jump times, the state space of the underlying Markov chain being the set of 4^N sample paths (or curves) \mathbf{C}_N introduced above.

This model is somehow a kind of discrete analogue of the Rouse chain [11], which is a popular model for polymer dynamics. There, each point of the chain is harmonically bound to its nearest neighbor, and move randomly in space. Some interesting statements can be made concerning the winding properties of such chains in 2d [12]. In this respect, from a probabilistic point of view, we keep in mind that winding variables are for Brownian curves, and they give rise to striking limit laws under convenient scalings (see e.g. [3, 4, 5]).

The paper is organized as follows. Section 2 presents the basic numerical and qualitative results, which rely on *ad hoc* discrete event simulation experiments together with a convenient graphical interface. In section 3, we propose several possible ways of coding the system with the related probabilistic descriptions (this section can be only glanced at without too much damage). The last part of the paper (section 4) contains the main quantitative results: relationships to exclusions models, scaling and thermodynamical limit, fluctuation analysis via theorems of central limit type.

2 Numerical experiments

2.1 Observations

We shall begin our study with several basic numerical observations. The model is purely stochastic and hence well-suited for Monte-Carlo simulations. These have been performed with the help of a graphical interface shown in Figure 2.2, which facilitates the exploration of the relevant parameter range, together with the display of the main regimes and phases of the system.

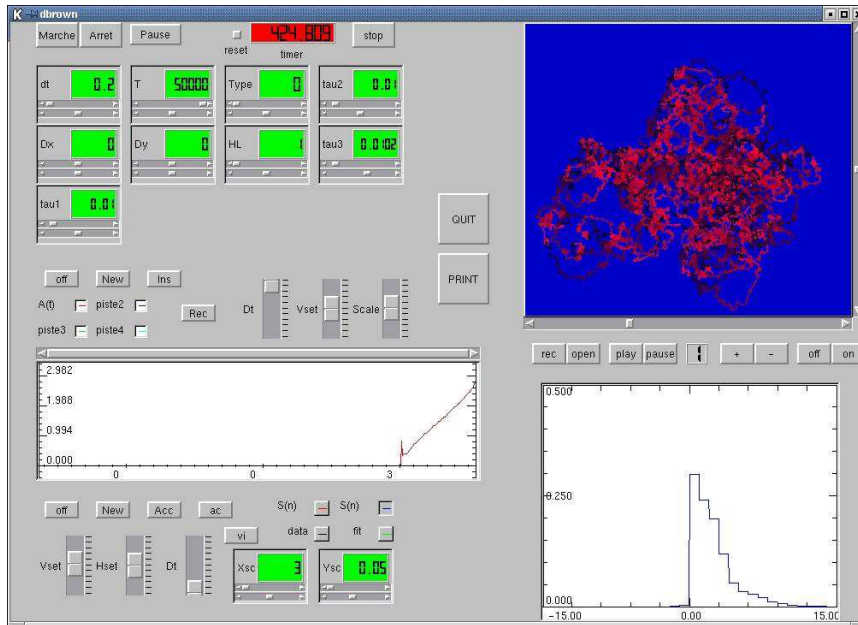


Fig. 2.2: Platform for numerical experiments.

Several parameters have to be tuned: the number of steps N ; the relative position of the extremities of the walk (D_x, D_y) ; the boundary conditions, which either can be defined to let the end points move independently, or can be fixed or to tied by some periodic boundary conditions; finally, the time constants associated with the elementary transformations, τ_1 with γ , τ_2 and τ_3 with λ^+ and λ^- . Any walk fulfilling these conditions is randomly generated at time $t = 0$ and then evolves

stochastically, with a movement depending on the rates and boundary conditions given above. After each new event, time is incremented by an amount inversely proportional to the number of all possible moves weighted by their respective rates. Interesting things happen when we break the chiral symmetry by imposing a *de-*

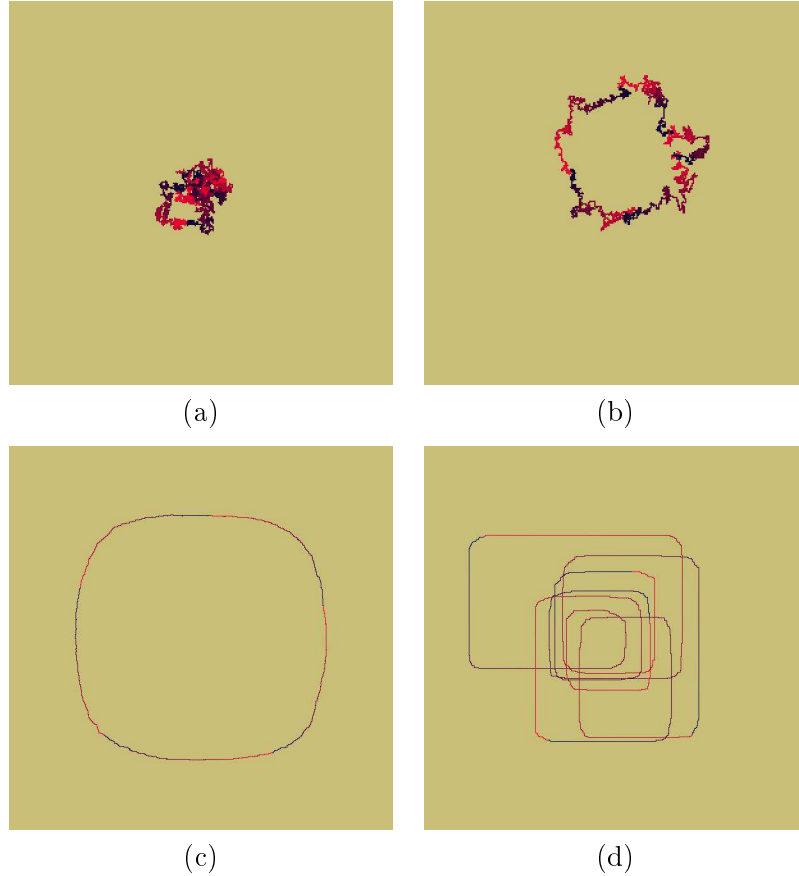


Fig. 2.3: Picture of a random walk of $N = 5000$ steps, showing the phases of the system for several values of η . Each colored segment represents 1000 steps. (a) $\eta = 0$ (the basic scale). (b) $\eta = 5$ (scale=1). (c) $\eta = 12.5$ (scale = 1/6). (d) $\eta = 250$ (scale = 1/2).

tuning between λ^+ and λ^- , in a proportion of order

$$\eta = N \frac{\lambda^+ - \lambda^-}{\lambda^+ + \lambda^-}. \quad (2.1)$$

For closed walks, four different situations can roughly be observed (see Figure 2.3).

- (a) $\eta \lesssim 1$. The initial configuration belongs to the equilibrium set of typical configurations, only fluctuations are altered by the finite value of η .
- (b) $1 \lesssim \eta \lesssim 6$. The system reaches an equilibrium which still corresponds to a random walk, the fractal dimension remaining equal to two, but a macroscopic circular drift is observed, yielding a sort of smoking ring.

- (c) $6 \lesssim \eta \lesssim 50$. The smoking ring gets stretched, and the elementary links becomes aligned over long distance. Fractal dimension shrinks to one, with the apparition of a long range order. Rotational invariance is broken.
- (d) $\eta \gtrsim 50$. The system is not able to reach its equilibrium. This typical configuration (out of equilibrium) exhibits an intricate hierarchical structure of bubbles. Smaller bubbles get evaporated into bigger bubbles. Time constants associated to these mechanisms grow exponentially with the size of the bubbles. Therefore, the final configuration corresponding to one bubble is never reached in the thermodynamic limit. We will refer to this non-equilibrium phase as a *glassy* phase.

2.2 Brownian windings

Some macroscopic random variables of interest can be constructed in order to be able to follow numerically the evolution of the system. First of all the total number of patterns $M1, M2, M3, M4$ is a set a variables which can be used to distinguish between a folded and a stretched phase of the system. All these number are expected to be fairly distributed in the folded phase although in the stretched phase we expect the pattern $M4$ to be in majority. In order to express mathematically the curling of the system, we consider variables related to the winding properties of planar Brownian curves, which are defined as follows: with each point in the plane is associated its *winding angle* θ , scanned by the random walker around this point. A

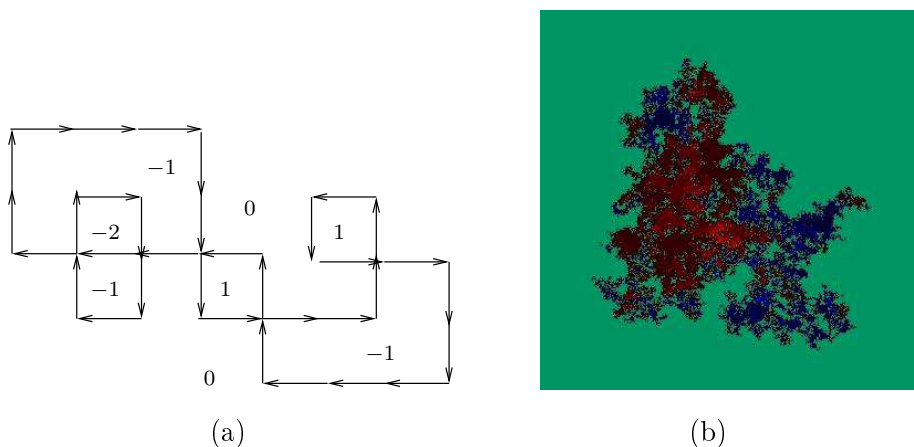


Fig. 2.4: Winding sectors defined for a closed random walk (a). Color gradient representing sectors for a walk of $N = 10^6$ steps: in red and blue, respectively, positive and negative winding sectors; in green, the null sector (b).

limit law for this variable has been derived by Spitzer for Brownian curves. Actually, assuming the length of the curve is set to $2\ell = Na^2$ when $N \rightarrow \infty$ and $a \rightarrow 0$ in the Brownian limit, the winding angle $\theta(\ell)$ of an arbitrary point has the asymptotic

probability [3]

$$\lim_{\ell \rightarrow \infty} P \left(\theta(\ell) = \frac{\alpha \log \ell}{2} \right) = \frac{1}{\pi} \frac{1}{1 + \alpha^2}.$$

For a closed walk, the value taken by θ are limited to $2n\pi$, where $n \in \mathbb{Z}$ represents the *winding number* associated with the point under consideration.

For each n , the set of points with the same winding number n form a *winding sector*, whose arithmetic area is a random variable denoted by $S_n(\ell)$. Under the

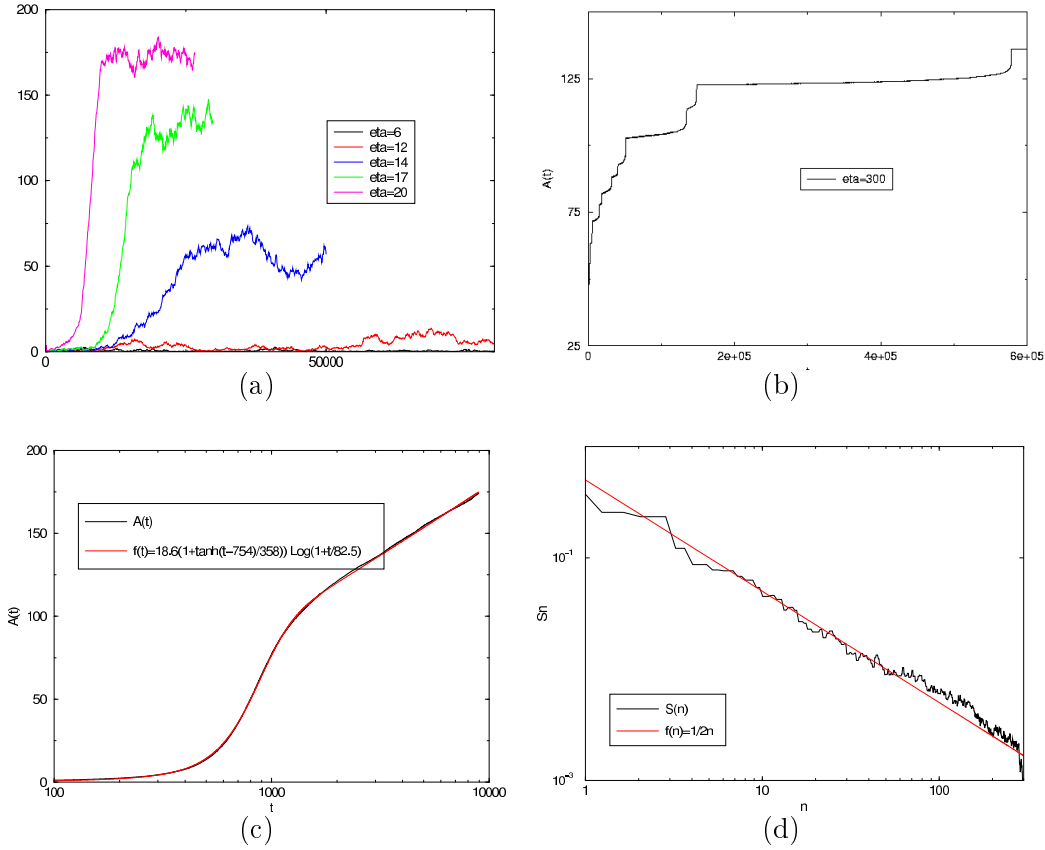


Fig. 2.5: Evolution of the total algebraic area (a,b,c). First transition with condensation in the first winding sector (a) $N = 1000$ steps. Unfolding transition with metastable states for $N = 2000$ steps (b). Curves (c) and (d), drawn in a logarithmic scale for $N = 10^6$, represent respectively the slow dynamics and the distribution of the S_n 's.

above mentioned Brownian limit for closed curves of length ℓ , we have [9]

$$\mathbb{E}[S_n(\ell)] = \frac{\ell}{2\pi n^2}.$$

In a similar way, the total *algebraic area* enclosed by the Brownian curve is defined as

$$A(\ell) = \sum_{n \in \mathbb{Z}} n S_n(\ell),$$

and its distribution is given by Lévy's law [4]

$$\lim_{\ell \rightarrow \infty} P(A(\ell) = 2s\ell) = \frac{\pi}{2 \cosh^2(\pi s)}.$$

The variable $S_n(\ell)$ is indeed enough for a complete characterization of the phases of the system.

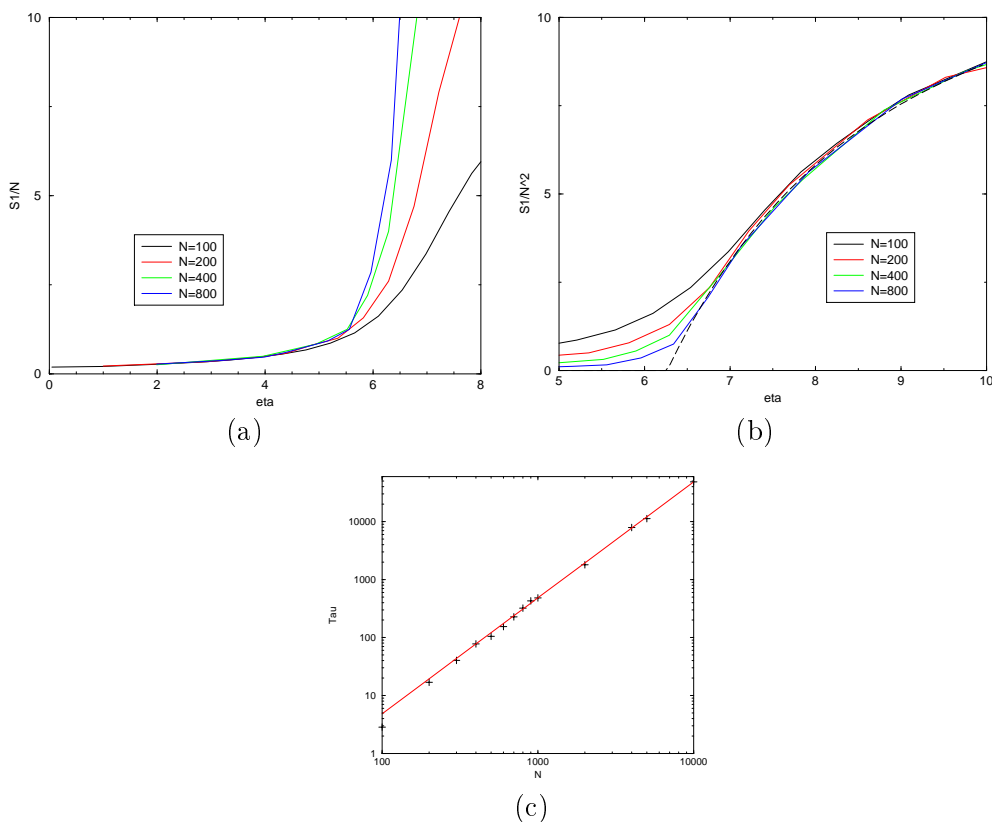


Fig. 2.6: The limit arithmetic area of the first winding sector when η varies, rescaled by N (a) and by N^2 (b). The dashed line in (b) is computed from part 4.3 giving the critical value $\eta_c = 2\pi$ separating the folded phases from stretched one. Scaling with N of time-constants for the transient regime (c) for $\eta = 10$; the fit gives a value 2.01 for the exponent.

2.3 Slow dynamics

The study of winding sectors and of associated variables is especially well adapted to describe the evolution of the system, since the presence of curls has a direct impact on the S_n distribution. A small but finite value of $\eta \lesssim 1$ will show itself by the existence of a shift in the distribution of S_n together with an unbalancing between positive and negative winding sectors. When $1 \lesssim \eta \lesssim 6$, the distribution of S_n condenses into either S_1 or S_{-1} . However, the behavior of S_1 or S_{-1} with regard to scaling factor does not change, and these variables still scale like N . The system reaches its stationary state after a transient regime characterized by a single time constant (Figure 2.5a). For $6 \lesssim \eta \lesssim 50$ the system get stretched, an unfolding transition occurs. S_1 or S_{-1} scale now like N^2 , and the fact that the walk is taut get reflected in the distribution of the motifs M_1, M_2, M_3, M_4 . When $\eta \gtrsim 50$ we obtained a glassy phase. This is related to the apparition of a hierarchy distribution of meta-stable configurations. The system evolves slowly to the rate of bubbles evaporations, small bubbles collapses and produce bubbles of bigger size. As a consequence, the transitory regime is completely different. For small size systems (see Figure 2.5b), it is observed that the total algebraic area increases by successive steps. These steps correspond to intermediate metastable states, consisting of bubbles of increasing size. The associated time constants behave roughly exponentially with the size of these bubbles. When $N \rightarrow \infty$ (see Figure 2.5c), a continuous spectrum of time constants is obtained and the convolution of these dynamical effect corresponding to different scale end up in a slow dynamical grows. The total algebraic area increases logarithmically with time. We observe also (see Figure 2.5d) that the distribution of S_n seems to have a limit characterized by the absence of negative (or positive) sectors, i.e. strictly zero for negative (or positive) index n , together with a scaling exponent around 1. Indeed this sequence of distributions seems to behave like n^{-1} , instead of n^{-2} for $\eta = 0$. Also the glassy transition is clearly of first order, with coexistence of a liquid phase (part of the walk which remains folded and disordered) and a solid glassy phase. The parameters corresponding to temperature and magnetization can be defined by analogy with standard spin glasses. They can be tuned independently, as we shall see later on, by letting vary η (which is roughly equivalent to the external magnetic field) and γ (pertaining in some sense to the temperature).

3 Sequence coding and generators: two formal approaches

3.1 A group decomposition

The dynamics of the system is Markovian. Its description involves a configuration space $\{\alpha\}$, a probability measure P_α and the generator $G_{\alpha\beta}$ of the evolution operator. Since the elementary transformations are local, and associated with each point of the random chain, G may be expressed as a sum of operators

$$G_{\alpha\beta} = \sum_{i=1}^N g_{\alpha\beta}(i),$$

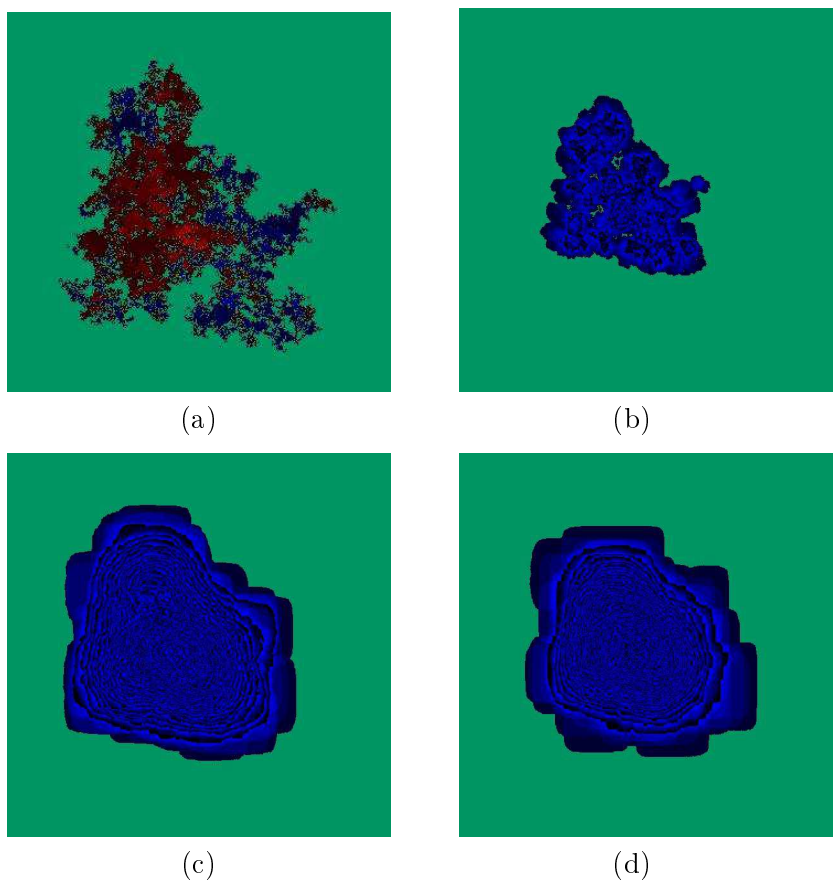


Fig. 2.7: First order glassy transition, with coexistence of a solid phase (on the edges) and a liquid phase (at the center). The scale is divided by a factor of 2 in (c) and of 4 in (d). The blue gradient indicates that all windings are negatives. A complete sequence of blue corresponds to an increase of 12 winding numbers.

Here it is to be understood that each $g(i)$ operates on a real space, endowed with the base $\{\omega_{\alpha_1}(1) \otimes \omega_{\alpha_2}(2) \dots \otimes \omega_{\alpha_N}(N)\}$ defined tensorially with respect to sites i , where each α_i stands for possible configurations at position i . Therefore, the sequence $\{\alpha_1, \dots, \alpha_N\}$ will generically denote a given configuration of the system. Then g has the following representation in the base of local operators

$$\begin{aligned}
 g(i) &= \lambda^+ \sigma^+(i)(1 - \sigma^-(i)) + \lambda^- \sigma^-(i)(1 - \sigma^+(i)) \\
 &+ \gamma^+(R(i) - R^4(i)) + \gamma^-(R^3 - R^4(i)),
 \end{aligned}$$

where $\sigma^+(i), \sigma^-(i), R(i), R^3(i)$ are the elementary operators corresponding to the transformations given in the introduction. They enjoy the following properties:

$$\begin{aligned}\sigma^\pm(i)^2 &= 0, \\ \sigma^\pm(i)\sigma^\mp(i)\sigma^\pm(i) &= \sigma^\pm(i), \\ \sigma^\pm(i)R(i) &= R(i)\sigma^\pm(i) = 0, \\ R^5(i) &= R(i).\end{aligned}$$

The fact that the transformations are local is illustrated by the commutation property

$$h(i)h(i+2) = h(i+2)h(i).$$

Many representations can be defined to encode system configurations. For example, we could take the sequence

$$\Omega_0 = \{z_1 = x + iy, z_2, \dots, z_N\}, \quad (z_i \in \mathbb{Z} + i\mathbb{Z})$$

formed by the affixes of the successive points in the plane, with the constraint that each point is separated from its neighbors by a single link. Another possible choice is

$$\Omega_1 = \{v_1 = z_2 - z_1, v_2 = z_3 - z_2, \dots, v_{N-1} = z_N - z_{N-1}\}, \quad (v_i \in \{1, i, -1, -i\}),$$

the set of successive links, which corresponds to the tangent map to Ω_0 . In this case, the center of gravity, i.e. the average over all point positions $z^* = (z_1 + \dots + z_N)/N$, defines equivalent classes. Then taking the tangent map to Ω_1 yields the sequence

$$\Omega_2 = \{u_1 = v_2 - v_1, u_2, \dots, u_{N-2} = v_{N-1} - v_{N-2}\},$$

which represents the patterns defined in introduction. In that case, the drift

$$v^* = (v_1 + \dots + v_{N-1})/N$$

depicts the separation between extremities, and may serve to define different equivalent classes. We will see later that, depending on the boundary conditions, z^* and v^* can be decoupled from the dynamics. In particular, this is true for periodic boundary conditions. Indeed Ω_2 should be the natural representation to express the dynamics of the system, since elementary transformations are performed on the patterns defined at each point of the chain. However, although any possible transition at a given point depends solely on the pattern of the point (for example a λ^+ -transition at point i can take place only if the walk performs a left bend at that point), the result of this transformation involves three successive patterns (for the event λ^+ , the pattern at i becomes a right bend, and both adjacent patterns at $i-1$ and $i+1$ are modified). On the other hand, in the Ω_1 representation, although each transition is conditioned by a pair of links, the result does modify only this pair.

We choose now Ω_1 to express G properly. As a site i of the chain has four possible configurations, depending on the orientation of the link v_i , let us introduce $\{\omega_0(i), \omega_1(i), \omega_2(i), \omega_3(i)\}$ the corresponding base in a *four*-dimensional space, and consider $\phi^{\alpha,\beta}(i)$, $\alpha, \beta \in \{0, 1, 2, 3\}$, the set of operators defined on this space by

$$\phi^{\alpha,\beta}\omega_\mu = \delta_{\beta\mu}\omega_\alpha.$$

In particular $\phi^{\alpha,\alpha}(i)$ is the projection onto the state ω_α at site i , the remainder of the sequence being left unmodified. With this notation, the generator takes the form

$$\begin{aligned} g(i) &= \lambda^+ [\phi^{\alpha+1,\alpha}(i)\phi^{\alpha,\alpha+1}(i+1) - \phi^{\alpha,\alpha}(i)\phi^{\alpha+1,\alpha+1}(i+1)] \\ &+ \lambda^- [\phi^{\alpha,\alpha+1}(i)\phi^{\alpha+1,\alpha}(i+1) - \phi^{\alpha+1,\alpha+1}(i)\phi^{\alpha,\alpha}(i+1)] \\ &+ \gamma^+ [\phi^{\alpha+1,\alpha}(i)\phi^{\alpha-1,\alpha}(i+1) - \phi^{\alpha,\alpha}(i)\phi^{\alpha+2,\alpha+2}(i+1)] \\ &+ \gamma^- [\phi^{\alpha,\alpha+1}(i)\phi^{\alpha,\alpha-1}(i+1) - \phi^{\alpha,\alpha}(i)\phi^{\alpha+2,\alpha+2}(i+1)], \end{aligned} \quad (3.1)$$

and commutation rules write

$$[\phi^{\alpha,\beta}(i), \phi^{\mu,\nu}(j)] = \delta_{ij} (\delta_{\beta\mu} \phi^{\alpha,\nu}(i) - \delta_{\alpha\nu} \phi^{\mu\beta}(i)).$$

The form (3.1) could be used to construct a transfer matrix representation [13]. For the moment, one can simply remark that the Lie algebra \mathcal{L} generated by the $\phi^{\mu\nu}$ is a \mathbb{Z}_2 -graded Lie algebra [20], so that it can be decomposed onto two Lie sub-algebras denoted by \mathcal{L}_0 and \mathcal{L}_1 , with the commutation relations

$$\begin{cases} [\mathcal{L}_0, \mathcal{L}_0] \subset \mathcal{L}_0, \\ [\mathcal{L}_0, \mathcal{L}_1] \subset \mathcal{L}_1, \\ [\mathcal{L}_1, \mathcal{L}_1] \subset \mathcal{L}_0. \end{cases}$$

This leads to introduce the following linear combinations

$$\kappa^{p,q} = \sum_{\alpha \in \{0,1,2,3\}} e^{\frac{i\pi p\alpha}{2}} \phi^{\alpha+q,\alpha}, \quad (3.2)$$

for $p, q \in \{0, 1, 2, 3\}$, with the commutation rules

$$[\kappa^{p,q}, \kappa^{p',q'}] = \left(e^{\frac{i\pi p q'}{2}} - e^{\frac{i\pi p' q}{2}} \right) \kappa^{p+p', q+q'},$$

where the sums $p+p'$ and $q+q'$ are taken modulo 4. One easily verifies that, when q varies, $\kappa^{0,q}$ and $\kappa^{2,q}$ generate \mathcal{L}_0 , while $\kappa^{1,q}$ and $\kappa^{3,q}$ generate \mathcal{L}_1 . In addition, from the very definition (3.2), the quantities

$$\begin{cases} Q_0 = \sum_j \kappa^{0,0}(j), \\ Q_1 = \sum_j \kappa^{1,0}(j), \\ Q_3 = \sum_j \kappa^{3,0}(j), \end{cases}$$

do commute with the generator. Later, by means of a more intuitive representation, we will be able to interpret the above formalism in terms of conservation of particles.

3.2 Chaos game representation

A way commonly used in DNA modeling ([15, 14] and references therein) in order to visualize dynamics in the configuration space consists in encoding the random

walk as an array of integers $\alpha_i \in \{0, 1, 2, 3\}$, $i \in \mathbb{N}$, and to associate with each sequence a complex number z , where

$$z = \sum_{p=0}^{N-1} \frac{1}{2^p} \exp(i\pi\alpha_p/2).$$

Graphically, this leads to the successive inclusion of disjoint square sectors representing the filtration defined by the random walk (see figure 3.8). To each random

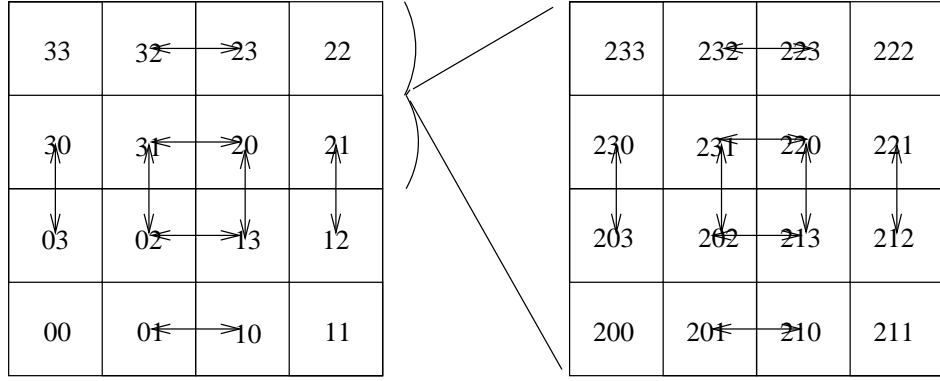


Fig. 3.8: Chaos Game representation of the first two links of the chain (left) and change of scale (right) representing the next link. Arrows indicate the transitions γ (center) and λ (on the edges).

walk of length N corresponds a square of area 4^{-N} centered at the related point z . There are exactly 4^N elementary squares and it becomes possible to define a discrete probability measure $\pi(z, t)$, constant on each such square, and whose evolution at time t is given by the forward Kolmogorov's equations

$$\frac{\partial \pi}{\partial t}(z, t) = \int dy \pi(y, t) g(y, z).$$

where $g(z, z')$ denotes the kernel of the infinitesimal generator in the above representation. Let g_0 be the part of the operator which operates at the upper level of the representation, that is on the first two links (see Figure 3.8), and let D the dilation operator mapping z onto $2z$. Then g writes

$$g = g_0 + Dg_0D^{-1} + D^2g_0D^{-2} + \dots$$

Moreover, as $N \rightarrow \infty$, g must satisfy the consistency relation

$$g = g_0 + DgD^{-1},$$

which can be split into two parts

$$g \stackrel{\text{def}}{=} g_1 + g_2,$$

where

$$\begin{cases} g_1 = g_0 + D^2g_1D^{-2}, \\ g_2 = Dg_0D^{-1} + D^2g_2D^{-2}. \end{cases}$$

It appears that g_1, g_2 can be easily diagonalized, since g_0 is diagonalizable and commutes with $D^2 g_0 D^{-2}$ and all higher order terms. Hence g_1, g_2 can be endowed with a simple tensorial structure which, in matrix form, reads

$$P_0 = \begin{array}{c} \begin{array}{cccc} 00 & 01 & 02 & 03 \\ 11 & 12 & 13 & 10 \\ 22 & 23 & 20 & 21 \\ 33 & 30 & 31 & 32 \end{array} \\ \begin{array}{|c|c|c|c|} \hline \begin{array}{c} [0] \\ [-\lambda^+] \\ [-\gamma] \\ [-\lambda^-] \end{array} & & \begin{array}{c} [\lambda^-] \\ [\gamma^-] \end{array} & \\ \hline \begin{array}{c} [\gamma^+] \\ [\lambda^+] \end{array} & \begin{array}{c} [0] \\ [-\lambda^+] \\ [-\gamma] \\ [-\lambda^-] \end{array} & & \begin{array}{c} [\lambda^+] \\ [\gamma^+] \end{array} \\ \hline & & \begin{array}{c} [0] \\ [-\lambda^+] \\ [\gamma^+] \\ [\lambda^+] \end{array} & \\ \hline \begin{array}{c} [\lambda^-] \\ [\gamma^-] \end{array} & & & \begin{array}{c} [0] \\ [-\lambda^+] \\ [\gamma^+] \\ [\lambda^+] \end{array} \\ \hline \end{array} \end{array} \begin{array}{l} 00 \\ 01 \\ 02 \\ 03 \\ 11 \\ 12 \\ 13 \\ 10 \\ 22 \\ 23 \\ 20 \\ 21 \\ 33 \\ 30 \\ 31 \\ 32 \end{array}$$

The self similarity is revealed by the fact that each 4×4 block element becomes 16×16 when one takes an additional link, in such a way that P_0 is added to itself in these blocks. The problem is intricate since g_1 and g_2 do not commute. When $\gamma^+ = \gamma^-$, P_0 can be diagonalized and its eigenvalues are 0 (9 times degenerated), $-(\lambda^+ + \lambda^-)$ (4 times degenerated), $-\gamma$ (twice degenerated) and -2γ (simple). These simple tensorial structure simply reflects the scale invariance in the chaos game representation or the translation invariance in the initial representation. When $N \rightarrow \infty$, it should be possible to exploit this symmetry to build an iterative map, aiming at generating the invariant measure or the self-organized critical one in the glassy phase. Before doing this, we will propose another formulation of the problem in terms of particle hops with exclusion.

4 Coupled exclusion models and thermodynamic limit

4.1 The mapping

In the last section, we used a representation helping to visualize the configuration space. There transitions between configurations were expressed as exchanges between square domains. We may go a bit farther on, using the fact that mutations are always either vertical or horizontal, and with opposite directions between both modified links (see Figure 4.9). This suggests indeed to recode each link j , $j = 1, \dots, N$ by means of two binary components $s_j^a \in \{0, 1\}$ and $s_j^b \in \{0, 1\}$ thus

establishing a *bijection* $\alpha_j \rightarrow (s_j^a, s_j^b)$ such that

$$\begin{cases} 0 \rightarrow (0, 0), \\ 1 \rightarrow (1, 0), \\ 2 \rightarrow (1, 1), \\ 3 \rightarrow (0, 1). \end{cases}$$

In this scheme a transition on a link does touch only either of its components. Indeed the infinitesimal generator is the sum of two terms: the first one acts on the sequence $\{s_i^a\}$, with rates conditioned by the sequence $\{s_i^b\}$ and vice-versa. We have thus a Markov process with state space

$$(S^a, S^b) = ((s_1^a, s_1^b), \dots, (s_N^a, s_N^b)),$$

a $2N$ -dimensional boolean vector. Then, for an arbitrary function $f : (S^a, S^b) \rightarrow \mathbb{C}$, the generator decomposes into

$$G = \sum_{i=1}^N h_a(i) + h_b(i), \quad (4.1)$$

where

$$\begin{aligned} h_a(i)f(S^a, S^b) &\stackrel{\text{def}}{=} \lambda_a^+(i) s_i^a \bar{s}_{i+1}^a [f((s_1^a, s_1^b), \dots, (0, s_i^b), (1, s_{i+1}^b), \dots, (s_N^a, s_N^b)) - f(S^a, S^b)] \\ &\quad + \lambda_a^-(i) \bar{s}_i^a s_{i+1}^a [f((s_1^a, s_1^b), \dots, (1, s_i^b), (0, s_{i+1}^b), \dots, (s_N^a, s_N^b)) - f(S^a, S^b)], \\ h_b(i)f(S^a, S^b) &\stackrel{\text{def}}{=} \lambda_b^+(i) s_i^b \bar{s}_{i+1}^b [f((s_1^a, s_1^b), \dots, (s_i^a, 0), (s_{i+1}^a, 1), \dots, (s_N^a, s_N^b)) - f(S^a, S^b)] \\ &\quad + \lambda_b^-(i) \bar{s}_i^b s_{i+1}^b [f((s_1^a, s_1^b), \dots, (s_i^a, 1), (s_{i+1}^a, 0), \dots, (s_N^a, s_N^b)) - f(S^a, S^b)], \end{aligned}$$

using the boolean notation $\bar{s} = 1 - s$. In order to express these generators in terms of local operators, let us define the following pairs of operators (a_j, a_j^\dagger) and (b_j, b_j^\dagger) : they leave unchanged the sample path, but the first [resp. the second] component of link j , and they are given by

$$\begin{aligned} a_j f(S^a, S^b) &\stackrel{\text{def}}{=} s_j^a f((s_1^a, s_1^b), \dots, (0, s_j^b), \dots, (s_N^a, s_N^b)), \\ b_j f(S^a, S^b) &\stackrel{\text{def}}{=} s_j^b f((s_1^a, s_1^b), \dots, (s_j^a, 0), \dots, (s_N^a, s_N^b)), \\ a_j^\dagger f(S^a, S^b) &\stackrel{\text{def}}{=} \bar{s}_j^a f((s_1^a, s_1^b), \dots, (s_j^a, 1), \dots, (s_N^a, s_N^b)), \\ b_j^\dagger f(S^a, S^b) &\stackrel{\text{def}}{=} \bar{s}_j^b f((s_1^a, s_1^b), \dots, (1, s_j^b), \dots, (s_N^a, s_N^b)). \end{aligned} \quad (4.2)$$

In terms of these operators, we also have (for (a) species)

$$h_a(i) = \lambda_a^-(i)(1 - a_i a_{i+1}^\dagger) a_i^\dagger a_{i+1} + \lambda_a^+(i)(1 - a_{i+1} a_i^\dagger) a_{i+1}^\dagger a_i.$$

Transition rates can be computed by inspecting the different cases, which yields the following expressions.

$$\begin{cases} \lambda_a^\pm(i) = \bar{s}_i^b \bar{s}_{i+1}^b \lambda^\mp + s_i^b s_{i+1}^b \lambda^\pm + \bar{s}_i^b s_{i+1}^b \gamma^\mp + s_i^b \bar{s}_{i+1}^b \gamma^\pm, \\ \lambda_b^\pm(i) = \bar{s}_i^a \bar{s}_{i+1}^a \lambda^\pm + s_i^a s_{i+1}^a \lambda^\mp + \bar{s}_i^a s_{i+1}^a \gamma^\pm + s_i^a \bar{s}_{i+1}^a \gamma^\mp. \end{cases} \quad (4.3)$$

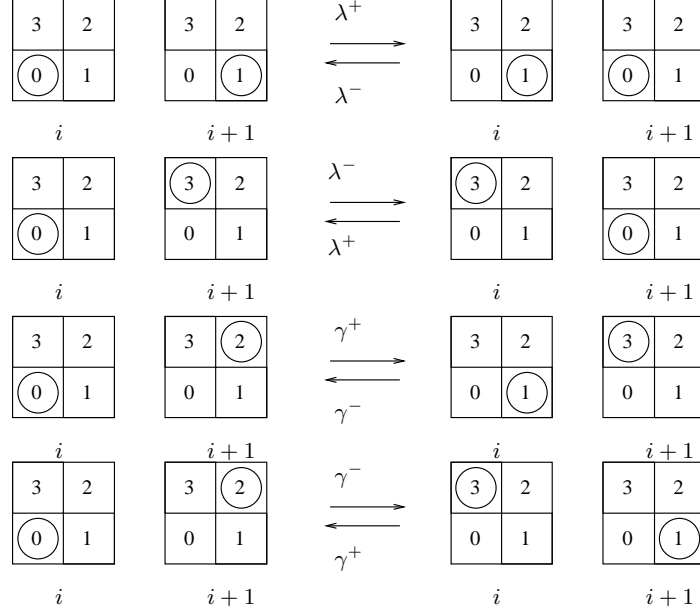


Fig. 4.9: Horizontal and vertical exchanges corresponding to transitions when link i has the value 0, according to the coding of section 3.2. Rules for other transitions follow by rotational symmetry.

The generator (4.1) represents two coupled systems of particles moving on a *one*-dimensional lattice with exclusion (i.e. there is at most one particle of each species per site [19]).

These particles perform random elementary jumps to the left or to the right. Obviously, both systems are interlaced: the jump rates $\lambda_a^\pm(i)$ of species (a) at site i are conditioned by the states of particles of species b at site $i, i+1$, and conversely according to relations (4.3). Setting

$$\begin{aligned} \lambda &\stackrel{\text{def}}{=} \frac{\lambda^+ + \lambda^-}{2} \quad \text{and} \quad \mu \stackrel{\text{def}}{=} \frac{\lambda^+ - \lambda^-}{2}, \\ \gamma &\stackrel{\text{def}}{=} \frac{\gamma^+ + \gamma^-}{2} \quad \text{and} \quad \delta \stackrel{\text{def}}{=} \frac{\gamma^+ - \gamma^-}{2}, \end{aligned} \quad (4.4)$$

(with similar definitions for λ_a, λ_b) the sub-generator of species (a) rewrites

$$\begin{aligned} h_a(i) &= \lambda_a(i)(a_i^\dagger - a_{i+1}^\dagger)(a_{i+1} - a_i) \\ &\quad + \mu_a(i) \left[a_i^\dagger(a_{i+1} - a_i) + (a_i^\dagger - a_{i+1}^\dagger)a_i \right] + V_a(i), \end{aligned}$$

where $\lambda_a(i)$ and $\mu_a(i)$ denote respectively the diffusion coefficient and the drift

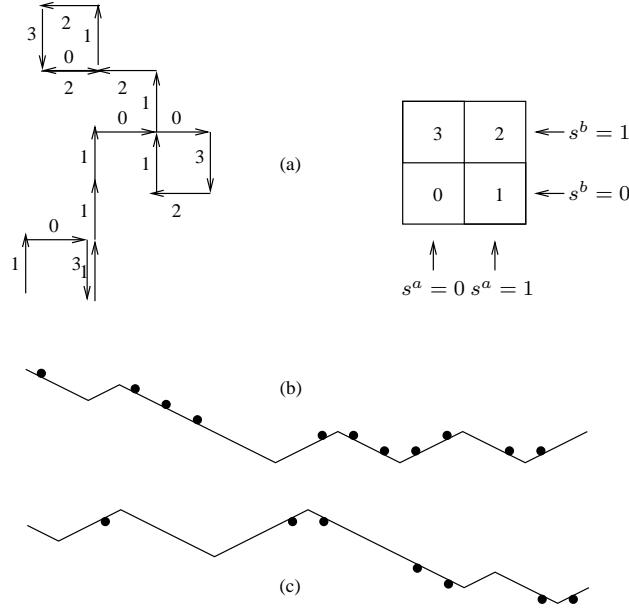


Fig. 4.10: Correspondence between chaos game representation of the random walk (a) and one-dimensional models of particle diffusion with exclusion. In (b), the sequence $\{s^a\}$ [resp. $\{s^b\}$] determines the profile of the diffusion [resp. the distribution of particles], drawn for $\gamma^\pm = \lambda^\pm$; in figure (c) the role of the particles has been exchanged.

(with the same notation as in (4.4)). After a routine algebra, we obtain

$$\begin{aligned}
 \lambda_a(i) &= \lambda + (\gamma - \lambda) (s_{i+1}^b - s_i^b)^2, \\
 \mu_a(i) &= \mu(1 - s_i^b - s_{i+1}^b) + \delta(s_{i+1}^b - s_i^b), \\
 \lambda_b(i) &= \lambda + (\gamma - \lambda) (s_{i+1}^a - s_i^a)^2, \\
 \mu_b(i) &= \mu(s_i^a + s_{i+1}^a - 1) + \delta(s_i^a - s_{i+1}^a).
 \end{aligned} \tag{4.5}$$

It is worth remarking λ_a and λ_b are strictly positive except when γ equals zero, in which case they might be zero at certain points. The interaction term takes the form

$$V_a(i) = 2\lambda_a(i)s_i^a s_{i+1}^a + s_i^a(\mu_a(i) - \mu_a(i-1)),$$

where $\mu_a(i)$ can be interpreted as a potential. A convenient representation of the system is to draw a one-dimensional profile from the sequence $\{s^b\}$ (positive or negative slope depending on whether s^b equals 0 or 1), to sketch the probabilistic inclination to turn left or right, as shown in Figures 4.10b, 4.10c.

In the particular case $\gamma^\pm = \lambda^\pm$, we get

$$\begin{cases}
 \lambda_a^\pm(i) = \frac{1}{2}(\lambda^+ + \lambda^-) \pm (s_i^b - \frac{1}{2})(\lambda^+ - \lambda^-), \\
 \lambda_b^\pm(i) = \frac{1}{2}(\lambda^+ + \lambda^-) \mp (s_i^a - \frac{1}{2})(\lambda^+ - \lambda^-),
 \end{cases} \tag{4.6}$$

and the sub-generator of species (a) takes the form

$$h_a(i) = \lambda a_i^\dagger (a_{i+1} + a_{i-1} - 2a_i) + \mu(2s_i^b - 1)(a_i^\dagger - a_{i+1}^\dagger)(a_i + a_{i+1}) + V_a(i),$$

where $V_a(i)$ is a diagonal term,

$$V_a(i) = \lambda s_i^a (s_{i+1}^a + s_{i-1}^a).$$

In this particular case, λ represents explicitly the diffusion constant of an isolated particle, with drift μ , the sign of which is determined by s_i^b . $V_a(i)$ is reminiscent of the interaction between particles coming from the exclusion constraint.

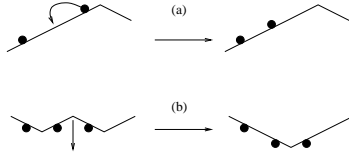


Fig. 4.11: (a) Elementary transition due to the jump of a type (a) particle, and the corresponding deformation of the profile defined by s^a (b) ($\gamma^\pm = \lambda^\pm$)

The distribution of particles labeled (a), submitted to the diffusion defined this way, is given by the sequence $\{s^a\}$ (0 or 1 particle depending on the individual site values of s_a). A complementary model is obtained by exchanging the roles of s^a and s^b . In addition, elementary transitions of the system correspond to jumps in the left or right direction of particles (a) and (b). In the complementary formulation, these transitions are materialized through modifications of the profile determined by s^a or s^b (see figure 4.11). Therefore, from this viewpoint, we can formulate the dynamic of subsystem (b) in terms of a KPZ model [17], in which the noise is produced by the distribution of particles (a). With this formulation, the conserved quantities (pointed out earlier) can be obtained in a straightforward manner, since they simply express conservation of particles. If boundary conditions are such that particles cannot escape from the system, the population of both species is conserved. This is for example the case when we impose periodic boundary conditions or also when extremities of the chain are fixed.

Suppose we fix the total amount n_a and n_b of particles (a) and (b), this results then on the random walk by the fact that $n_0 + n_3 = n_a$ and $n_0 + n_1 = n_b$ are fixed (n_i is the number of links i). Since $n_0 + n_1 + n_2 + n_3 = N$ it then easy to convince oneself that this is equivalent to fix $n_0 - n_2$ and $n_1 - n_3$, which is enough to determine the respective positions of the initial and final points of the walk.

In addition, except when $\gamma = 0$, we get an easy way to determine the irreducible classes of the system. In fact, for closed systems with a fixed number of particles, once the population of each species is fixed, just start from the configuration (11..1100..00) for both species where all particles have been disposed to the left. Then, owing to possible consecutive jumps to the right, which for $\gamma \neq 0$ are always authorized, one can reach any arbitrary configuration. This shows that for closed systems irreducible classes are indexed by the number of particles in each species, which corresponds to the separation between the extremities of the walk. On

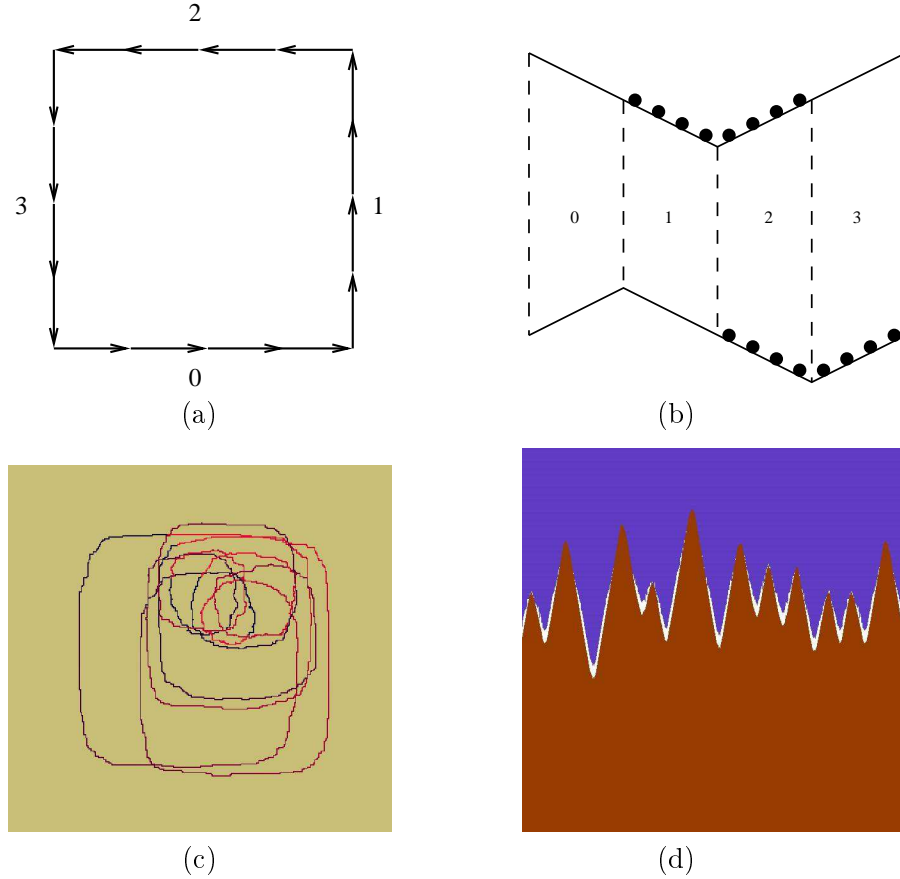


Fig. 4.12: (a) Stable configuration for closed chains. (b) Corresponding representation in terms of exclusion models. (c) Glassy state with $N = 5000$. (d) Corresponding KPZ landscape with the density of trapped particles represented in white.

the other hand, for open sample paths with free boundary conditions, irreducibility holds as long as particles can both enter and leave the system. An interesting point is the way stable configurations, which are numerically observed, are represented by means of this exclusion process formulation. In agreement with the intuition, Figure 4.12 depicts a stable situation where particles are trapped in a well. As this remains true with the complementary representation (see the lower part of Figure 4.12b), the following iterative scheme could be used to generate the global invariant measure: let particles (a) evolve assuming the dynamics of particles (b) is frozen; then, once this *conditional* stationary regime is reached, switch to particles (b) conditioned by particles (a), etc. Translated mathematically, we proposed the following iterative scheme in order to capture the invariant measure

$$\begin{aligned}
 X^{n+1} &= \lim_{t \rightarrow \infty} \mathbb{E} (S^a(t) \mid S^b(t) = Y^n, S^a(0) = X^n), \\
 Y^{n+1} &= \lim_{t \rightarrow \infty} \mathbb{E} (S^b(t) \mid S^a(t) = X^n, S^b(0) = Y^n).
 \end{aligned}$$

Numerically, the sequences of random variables X^n and Y^n seemingly converge for $\eta < 50$ to the stationary variables $S^a(\infty)$ and $S^b(\infty)$.

Up to an abuse of notation, we shall often identify the random process with any of its sample paths. For instance we shall simply write $P(S^a | S^b)$ [resp. $P(S^b | S^a)$] the conditional invariant measure of particles (a) [resp. (b)] when the dynamics of particles (b) is frozen. Then the iterative scheme can be reformulated as

$$\begin{aligned} P_{n+1}(S^a) &= \sum_{\{S^b\}} P(S^a | S^b) Q_n(S^b) \\ Q_{n+1}(S^b) &= \sum_{\{S^a\}} P(S^b | S^a) P_n(S^a) \end{aligned}$$

where P_n [resp. Q_n] represents the probability measure of the S^a [resp. S^b] after n steps. If this iteration converges, the joint probability for the invariant measure will be given by

$$P(S^a, S^b) = P(S^a | S^b) Q(S^b) = P(S^b | S^a) P(S^a)$$

in case these two expressions coincide.

4.2 Conditional equilibrium

4.2.1 The case of a stretched walk

Let us have a look to a special case which can be solved exactly. It will provide some hints about scaling of the parameters when $N \rightarrow \infty$.

Consider a random walk with fixed extremities, and consisting only of links oriented either to the north or to the east, i.e. $(\alpha_i \in \{0, 1\}, i = 1 \dots N)$. Here folds do not

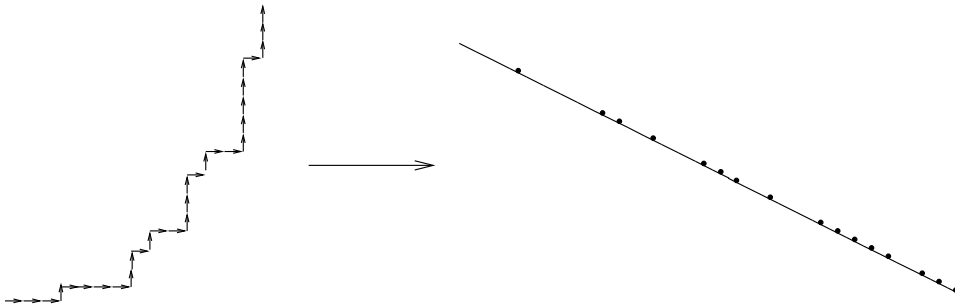


Fig. 4.13: Stretched random walk and asymmetric exclusion process.

exist (see figure (4.13)), so that $s^b = 0$ everywhere and solely transitions λ^\pm take place. It turns out that the invariant measure has the product-form

$$P(\alpha_1, \dots, \alpha_N) = p_{\alpha_1} p_{\alpha_2} \dots p_{\alpha_N}.$$

Indeed, introducing the occupation rate of particles (a) $q_i = p_1(i) = 1 - p_0(i)$, we have the balance equations

$$\lambda^+(1 - q_i)q_{i+1} = \lambda^-q_i(1 - q_{i+1}). \quad (4.7)$$

Setting

$$r_i \stackrel{\text{def}}{=} \frac{q_i}{1 - q_i},$$

we obtain a geometric series

$$r_i = r_0 \left(\frac{\lambda^-}{\lambda^+} \right)^i = r_0 \exp \left[i \log \frac{1 - \eta/N}{1 + \eta/N} \right]. \quad (4.8)$$

In (4.8), the ratio

$$\frac{\eta}{N} = \frac{\lambda^+ - \lambda^-}{\lambda^+ + \lambda^-} = \frac{\mu}{\lambda},$$

already introduced in (2.1) and (4.4), gives the *typical scale* $n_c \simeq \frac{N}{\eta}$, above which we obtain straight aligned patterns. Here r_0 is a normalizing constant, which permits to fix the expected value D_0 of the particle density

$$\nu = \frac{1}{N} \sum_{i=1}^N \mathbb{1}_{\{\alpha_i=1\}},$$

that is

$$D_0 = \mathbb{E}(\nu) = \frac{1}{N} \sum_{i=1}^N q_i = \frac{1}{N} \sum_{i=1}^N \frac{r_i}{1 + r_i}.$$

Letting $N \rightarrow \infty$, we analyze the limiting process under the *scaling*,

$$\eta \stackrel{\text{def}}{=} \lim_{N \rightarrow \infty} \frac{N\mu}{\lambda}, \quad (4.9)$$

where η , up to some abuse in the notation, is now a parameter independent of N . This is tantamount to assume that μ is implicitly a function of N .

Fixing $x = i/N$ and taking the expansion with respect to η/N in (4.8), we get the limit equation

$$r(x) = r_0 \exp(-2\eta x), \quad (4.10)$$

which implies in turn

$$D_0 = \int_0^1 dx \left(1 - \frac{1}{1 + r_0 \exp(-2\eta x)} \right) = \frac{1}{2\eta} \log \frac{1 + r_0}{1 + r_0 \exp(-2\eta)}.$$

Consequently,

$$r_0 = \frac{\sinh(\eta D_0)}{\sinh \eta(1 - D_0)} e^\eta.$$

The integral of the particle density, taken as a function of x , is shown in Figure 4.13 and is given by

$$h(x) = \int_0^x du \left(1 - \frac{1}{1 + r_0 \exp(-2\eta u)} \right) = \frac{1}{\eta} \log \left[\frac{1 + r_0}{1 + r_0 \exp(-2\eta x)} \right].$$

This asymmetric exclusion model can be solved under more general conditions, in particular with open boundaries, using matrix methods [21]. The above simple example confirms the observed fact that the correct scaling parameter is indeed η , and also somehow explains why the chain remains Brownian when $\eta \lesssim 1$.

4.2.2 The general case

Once the sequence $\{s^b\}$ is given, particles (a) form a unidimensional exclusion process in an inhomogeneous environment. Its transition rates to the right or to the left at position i have been given in (4.3).

Our basic claim is that the reasoning of section 4.2.1 still holds for a closed system where the number of particles is kept constant. Exactly this means that, as long as there is no *current* in the system, conditional detailed balance equations of type (4.7) are still valid at steady state, just replacing λ^\pm by $\lambda_a^\pm(i)$.

We present no proof of this fact (which could likely be obtained by coupling arguments), and write brutally the equilibrium equations

$$\lambda_a^+(i)(1 - q_i^a)q_{i+1}^a = \lambda_a^-(i)q_i^a(1 - q_{i+1}^a), \quad i = 1 \dots N,$$

where sites $N + 1$ and 1 are identified for periodic boundary conditions, and q_i^a [resp. q_i^b] is the random variable equal to the conditional probability of having one particle of type (a) [resp. (b)] in position i given the sequence $\{s^b\}$ [resp. $\{s^a\}$], that is

$$q_i^a = \mathbb{E}[s_i^a | S^b], \quad q_i^b = \mathbb{E}[s_i^b | S^a]. \quad (4.11)$$

Setting

$$r_i^a \stackrel{\text{def}}{=} \frac{q_i^a}{1 - q_i^a},$$

we obtain

$$\log[r_{i+1}^a] - \log[r_i^a] = \log\left(\frac{\lambda_a^-(i)}{\lambda_a^+(i)}\right). \quad (4.12)$$

By using (4.3), an easy algebra based on the boolean character of the s_i^b yields

$$\log \frac{\lambda_a^-(i)}{\lambda_a^+(i)} = (1 - 2s_i^b) \log \frac{\lambda - \mu}{\lambda + \mu} + (s_{i+1}^b - s_i^b) \log \frac{(\gamma - \delta)(\lambda + \mu)}{(\gamma + \delta)(\lambda - \mu)}, \quad (4.13)$$

with a similar equation for type b particles. In addition we observe that the constraints

$$r_{N+1}^a = r_1^a, \quad r_{N+1}^b = r_1^b,$$

for periodic boundary conditions, will be automatically fulfilled as long as the system of particles (b) is globally neutral (i.e. particles and holes have the same cardinality), in which case

$$\sum_{i=1}^N (1 - 2s_i^b) = 0.$$

4.3 Closed curves: weak convergence for large N

We will now combine the stationary product forms obtained for each particle species, according to the iterative scheme proposed at the end of section 4.1. Throughout this section, the dependence on N of the random variables q_k^a, q_k^b , given by (4.11), is kept implicit for the sake of shortness in the notation.

Introduce $\{w_i^a, i \geq 0\}$ and $\{w_i^b, i \geq 0\}$, two families of independent and identically distributed Bernoulli random variables with parameter $1/2$ and values $\{1, -1\}$. Without further comment, we assume that $(S^a, S^b), \{w_i^a, i \geq 0\}, \{w_i^b, i \geq 0\}$ are defined on the same probability space.

Lemma 4.1. *Let $\alpha_k, k \geq 1$, denote a sequence of complex numbers satisfying the condition $\sup_k |\alpha_k| < \infty$.*

There exists a probability space such that

$$\begin{cases} \frac{1}{N} \sum_{k=1}^N \alpha_k s_k^a = \frac{1}{N} \sum_{k=1}^N \alpha_k (q_k^a + \sigma_k^a w_k^a) + O(N^{-2}) & a.s., \\ \frac{1}{N} \sum_{k=1}^N \alpha_k s_k^b = \frac{1}{N} \sum_{k=1}^N \alpha_k (q_k^b + \sigma_k^b w_k^b) + O(N^{-2}) & a.s., \end{cases} \quad (4.14)$$

where

$$\sigma_k^a = \sqrt{q_k^a(1 - q_k^a)}, \quad \sigma_k^b = \sqrt{q_k^b(1 - q_k^b)}, \quad \forall k \geq 1. \quad (4.15)$$

Proof. The starting point is the straightforward decomposition of the probability measure $P(S^a, S^b)$ as

$$P(S^a, S^b) = P(S^a | S^b)P(S^b) = P(S^b | S^a)P(S^a).$$

Considering the invariant measure of the process $(S^a(t), S^b(t))$, we claim the conditional probabilities $P(S^a | S^b)$ and $P(S^b | S^a)$ coincide with the equilibrium probabilities obtained in the last section *for each particle species*. In the present situation, this is tantamount to writing the equation

$$P(S^a | S^b) = \prod_{i=1}^N (s_i^a q_i^a + \bar{s}_i^a (1 - q_i^a)),$$

where the q_i^a 's depend implicitly of S^b . To analyze more precisely the coupling between the two families, we introduce the Laplace transforms

$$\varphi_k^a(\alpha) \stackrel{\text{def}}{=} \mathbb{E} \left[\exp \left\{ \frac{1}{N} \sum_{k=1}^N \alpha_k s_k^a \right\} \right] = \mathbb{E} \left[\prod_{k=1}^N [1 + q_k^a (e^{\frac{\alpha k}{N}} - 1)] \right].$$

Then

$$\varphi_k^a(\alpha) = \mathbb{E} \left[\exp \left\{ \frac{1}{N} \sum_{k=1}^N \alpha_k q_k^a + \frac{1}{2N^2} \sum_{k=1}^N \alpha_k^2 q_k^a (1 - q_k^a) + O\left(\frac{1}{N^2}\right) \right\} \right].$$

On the other hand, starting from the equality

$$\mathbb{E} \left[\exp \left\{ \frac{1}{N} \sum_{k=1}^n \alpha_k (q_i^a + \sigma_i^a w_i^a) \right\} \right] = \mathbb{E} \left[\exp \left\{ \frac{1}{N} \sum_{k=1}^N \alpha_k q_k^a + \sum_{k=1}^N \log \cosh \frac{\sigma_k^a \alpha k}{N} \right\} \right],$$

with regard to the (a) species, we observe that the value of σ_k^a given in (4.15) gives the matching

$$\mathbb{E} \left[\exp \left\{ \frac{1}{N} \sum_{k=1}^N \alpha_k s_k^a \right\} \right] = \left[\mathbb{E} \exp \left\{ \frac{1}{N} \sum_{k=1}^N \alpha_k (q_k^a + \sigma_k^a w_k^a) + O\left(\frac{1}{N^2}\right) \right\} \right]. \quad (4.16)$$

Since all random variables at stake are uniformly bounded, equation (4.16) yields at once (4.14), but only in distribution. To conclude the proof of the lemma, we make use of transfer and coupling theorems due to Skorohod and Dudley (see [16], theorem 4.30 and corollaries 6.11, 6.12), which allow to switch from equalities in distribution to almost sure properties, since on the original probability space the right member of system (4.14) is a measurable mapping of the left one. ■

4.3.1 Fundamental scaling, thermodynamic limit and fluctuations

For any i , $1 \leq i \leq N$, we put ad libitum $x = i/N$, $0 \leq x \leq 1$.

Proposition 4.2. *Under the fundamental scaling*

$$\begin{cases} \frac{\mu}{\lambda} = \frac{\eta}{N} + o\left(\frac{1}{N}\right), \\ \frac{\delta}{\gamma} = O\left(\frac{1}{N}\right), \end{cases}$$

the weak limits

$$\rho^a(x) = \lim_{N \rightarrow \infty} q_{xN}^a \quad \text{and} \quad \rho^b(x) = \lim_{N \rightarrow \infty} q_{xN}^b \quad (4.17)$$

exist and satisfy the autonomous system of deterministic nonlinear differential equations

$$\begin{cases} \frac{\partial \rho^a(x)}{\partial x} = 4\eta \rho^a(x)(1 - \rho^a(x))\left(\rho^b(x) - \frac{1}{2}\right), \\ \frac{\partial \rho^b(x)}{\partial x} = -4\eta \rho^b(x)(1 - \rho^b(x))\left(\rho^a(x) - \frac{1}{2}\right). \end{cases} \quad (4.18)$$

In addition, the assumed closure of the original random walk imposes the relations

$$\begin{cases} \int_0^1 \rho^a(x) dx = \int_0^1 \rho^b(x) dx = \frac{1}{2}, \\ \rho^a(x+1) = \rho^a(x), \\ \rho^b(x+1) = \rho^b(x). \end{cases} \quad (4.19)$$

Proof. Taking the expansion with respect to N in equations (4.12) and (4.13), and using lemma 4.1, we get after some algebra

$$\begin{cases} \log \frac{r_1^a}{r_1^a} = \frac{2\eta}{N} \sum_{j=1}^{k-1} (2q_j^b + 2\sigma_j^b w_j^b - 1) + O\left(\frac{1}{N}\right) \quad a.s., \\ \log \frac{r_1^b}{r_1^b} = -\frac{2\eta}{N} \sum_{j=1}^{k-1} (2q_j^a + 2\sigma_j^a w_j^a - 1) + O\left(\frac{1}{N}\right) \quad a.s. \end{cases} \quad (4.20)$$

Since N is a parameter and x rather stands for a variable, it is be convenient to introduce the following functions of x

$$q_N^a(x) \stackrel{\text{def}}{=} q_{[xN]}^a, \quad r_N^a(x) \stackrel{\text{def}}{=} \frac{q_N^a(x)}{1 - q_N^a(x)}, \quad \sigma_N^a(x) \stackrel{\text{def}}{=} \sqrt{q_N^a(x)(1 - q_N^a(x))},$$

and similarly for the (b) species.

To omit some tedious technicalities, we will only sketch the remaining lines of the proof.

First, it is not difficult to see that by restricting the expansion in (4.16) up to terms of order N^{-1} , and using the definition of r_k^a, r_k^b , we come to the simplified system

$$\left\{ \begin{array}{l} q_k^a = \frac{r_1^a \exp\left[\frac{2\eta}{N} \sum_{j=1}^{k-1} (2q_j^b - 1)\right]}{1 + r_1^a \exp\left[\frac{2\eta}{N} \sum_{j=1}^{k-1} (2q_j^b - 1)\right]} + O\left(\frac{1}{N}\right) \quad a.s., \\ q_k^b = \frac{r_1^b \exp\left[-\frac{2\eta}{N} \sum_{j=1}^{k-1} (2q_j^a - 1)\right]}{1 + r_1^b \exp\left[-\frac{2\eta}{N} \sum_{j=1}^{k-1} (2q_j^a - 1)\right]} + O\left(\frac{1}{N}\right) \quad a.s. \end{array} \right. \quad (4.21)$$

In a second step, it can be shown from (4.21), as in a purely deterministic context, that the quantities $q_N^a(x), q_N^b(x)$, form Cauchy sequences, hence converging, for all $0 \leq x \leq 1$. To see that the deterministic limits (4.17) exist and satisfy (4.18) is straightforward by approximating discrete sums by Riemann's integrals. This yields the differential system

$$\left\{ \begin{array}{l} \frac{\partial}{\partial x} \left[\log \frac{\rho^a(x)}{1 - \rho^a(x)} \right] = 2\eta(2\rho_b(x) - 1), \\ \frac{\partial}{\partial x} \left[\log \frac{\rho^b(x)}{1 - \rho^b(x)} \right] = -2\eta(2\rho_a(x) - 1), \end{array} \right.$$

which has similarities with the famous Lotka-Volterra equations, where x plays here the role of the time. It is worth noting that (4.10) is immediately revisited, taking merely $\rho^b(x) \equiv 0$ (i.e. the density of particles (b) is kept constant). ■

It is also tempting to get some insight into fluctuations around the above deterministic limit. This will be achieved by establishing the forthcoming central limit theorem.

Proposition 4.3. *Under the fundamental scaling, the weak limits*

$$g^a(x) = \lim_{N \rightarrow \infty} \sqrt{N} \frac{q_N^a(x) - \rho^a(x)}{\sigma_a^2(x)}, \quad g^b(x) = \lim_{N \rightarrow \infty} \sqrt{N} \frac{q_N^b(x) - \rho^b(x)}{\sigma_b^2(x)}, \quad (4.22)$$

exist and satisfy the system of stochastic differential equations

$$\left\{ \begin{array}{l} dg^a(x) = 4\eta \left[\sigma_a^2(x) g^b(x) dx + \sigma_b(x) dW^b(x) \right], \\ dg^b(x) = -4\eta \left[\sigma_b^2(x) g^a(x) dx + \sigma_a(x) dW^a(x) \right], \end{array} \right. \quad (4.23)$$

where

$$\sigma_a(x) \stackrel{\text{def}}{=} \sqrt{\rho^a(x)(1 - \rho^a(x))}, \quad \sigma_b(x) \stackrel{\text{def}}{=} \sqrt{\rho^b(x)(1 - \rho^b(x))}.$$

Proof. Letting

$$X_N^a(x) \stackrel{\text{def}}{=} \frac{1}{\sqrt{N}} \sum_{k=1}^{\lfloor xN \rfloor} w_k^a, \quad X_N^b(x) \stackrel{\text{def}}{=} \frac{1}{\sqrt{N}} \sum_{k=1}^{\lfloor xN \rfloor} w_k^b,$$

we consider the two white noise processes

$$W^a(x) \stackrel{\text{def}}{=} \lim_{N \rightarrow \infty} X_N^a(x), \quad W^b(x) \stackrel{\text{def}}{=} \lim_{N \rightarrow \infty} X_N^b(x).$$

We call on a strong approximation theorem, which is a refinement of the invariance principle (see [18]: it shows how to construct $W^a(x)$ and $W^b(x)$ on the same probability space as X_N^a and X_N^b) in such a way that

$$\sup_{0 \leq x \leq 1} |X_N(x) - W(x)| = O\left(\frac{\log N}{\sqrt{N}}\right).$$

Arguing as in the derivation of proposition 4.2, we can write

$$\begin{cases} \log \frac{r_N^a(x)}{r_N^a(0)} = 2\eta \int_0^x du (2q_N^b(x) - 1) + \frac{4\eta}{\sqrt{N}} \int_0^x \sigma_N^b(u) dW^b(u) + O\left(\frac{\log N}{N}\right), \\ \log \frac{r_N^b(x)}{r_N^b(0)} = -2\eta \int_0^x du (2q_N^a(x) - 1) - \frac{4\eta}{\sqrt{N}} \int_0^x \sigma_N^a(u) dW^a(u) + O\left(\frac{\log N}{N}\right), \end{cases} \quad (4.24)$$

where the stochastic integrals are taken in the Itô sense (see [22]). Defining $g_N^a(x)$ and $g_N^b(x)$ by the equations

$$\begin{aligned} q_N^a(x) &= \rho^a(x) + \sigma_a^2(x) g_N^a(x), \\ q_N^b(x) &= \rho^b(x) + \sigma_b^2(x) g_N^b(x), \end{aligned}$$

then putting these expressions into (4.24) and differentiating (4.24) (details are omitted), we are lead to (4.24). The proof of proposition 4.3 is completed. \blacksquare

Remark Let us comment on the scaling of δ . Contrary to the scaling of μ , which is naturally dictated by homogeneity (the sums in (4.20) remain meaningful after dividing by N , when $N \rightarrow \infty$), it is a purely dynamical consideration which dictates the scaling of δ . Indeed, μ and δ are associated to time constants τ_μ and τ_δ . The quantity τ_μ represents the typical unit of time for a free particle (a) or (b) to drift along the system over a finite distance, whereas τ_δ is a time-scale for rotations of vertical or horizontal fold $M2$ of the chain, remembering that δ stands for the *detuning* between γ^+ and γ^- defined in section 1. Therefore either these time-scale are coherent and δ is rescaled, otherwise rotational motions of $M2$ occur at a shorter time scale and a different analysis has to be conducted, since motifs $M2$ (which correlate hole-particle pairs of species (a) and (b)) reach their equilibrium distribution before particles have enough time to move along the system. Numerically we could not perceive any specific effect related to δ , so that we restricted ourselves to the above *fundamental scaling*.

4.3.2 Second order phase transition

Here we focus on on the deterministic (4.18) part of the equations. Using the notation

$$\nu_a(x) \stackrel{\text{def}}{=} 2\rho^a(x) - 1, \quad \nu_b(x) \stackrel{\text{def}}{=} 2\rho^b(x) - 1,$$

apart from the trivial solution $\nu_a(x) = \nu_b(x) = 0$, we obtain from (4.18)

$$\frac{\nu_a(x)}{1 - \nu_a^2(x)} \frac{\partial \nu_a(x)}{\partial x} = - \frac{\nu_b(x)}{1 - \nu_b^2(x)} \frac{\partial \nu_b(x)}{\partial x},$$

or, after integration,

$$1 - \nu_a^2(x) = \frac{C}{1 - \nu_b^2(x)}, \quad 0 < C < 1,$$

since $|\nu_a| < 1$ and $|\nu_b| < 1$. Plugging the last relation into (4.18) leads to

$$\left(\frac{\partial \nu_a(x)}{\partial x} \right)^2 = \eta^2 [1 - \nu_a^2(x)] [1 - C - \nu_a^2(x)], \quad (4.25)$$

the solution of which is the standard Jacobi elliptic function

$$\nu_a(x) = \frac{1}{\sqrt{1-C}} \operatorname{sn}(\eta x, \sqrt{1-C}).$$

Finding the constant C is equivalent to compute the fundamental period of these functions. Hence, denoting by $X(C)$ the period of $\nu_a(x)$, we have solve

$$X(C) = 1. \quad (4.26)$$

From (4.25) we see that $\nu_a(x)$ is bounded by $-\sqrt{1-C}$ and $\sqrt{1-C}$. Taking into account the constraint $(\int_0^1 \nu_a(x) dx = 0)$, $X(C)$ is exactly given by

$$X(C) = \frac{1}{\eta} F\left(\frac{\pi}{2}, \sqrt{1-C}\right) = \frac{4}{\eta} \int_0^1 \frac{d\nu}{\sqrt{[1-\nu^2][1-(1-C)\nu^2]}},$$

where F is the standard elliptic integral of first kind.

$X(C)$ is a decreasing function of C on $]0, 1]$, reaching its minimum for $C = 1$, so that

$$X(C) \geq X(1) = \frac{2\pi}{\eta}.$$

Thus appears is a *critical value* for η , namely

$$\eta_c = 2\pi.$$

When $\eta_c < 2\pi$, (4.26) cannot be fulfilled and we are left with the trivial solution.

When $\eta_c \geq 2\pi$, it is straightforward to compute the arithmetic area $S_1(\eta)$ of the first winding sector, since it is indeed the only non-vanishing sector. Setting

$$\begin{cases} h_x(u) = \frac{1}{2} \int_0^u dv [\nu_a(v) + \nu_b(v)] dv, \\ h_y(u) = \frac{1}{2} \int_0^u dv [\nu_a(v) - \nu_b(v)] dv, \end{cases}$$

$S_1(\eta)$ is simply the area enclosed by the curve $(h_x(u), h_y(u))$ $u \in [0, 1]$, which is given by

$$S_1(\eta) = \frac{1}{2} \int_0^1 du \left[h_x \frac{\partial h_y}{\partial u} - h_y \frac{\partial h_x}{\partial u} \right],$$

or, after some algebra,

$$S_1(\eta) = \frac{1}{2\eta^2} \int_0^{\sqrt{1-C}} \frac{\nu}{\sqrt{(1-\nu^2)(1-C-\nu^2)}} \log \left[\frac{1+\nu}{1-\nu} \right] d\nu,$$

keeping in mind that C is also a function of η . The corresponding curve displayed in figure 2.6.b matches pretty nicely all numerical observations, in particular with regard to the critical value η_c .

4.3.3 More about fluctuations for $\eta < \eta_c$

When η is under the threshold η_c , the deterministic part becomes trivial, and we are left with fluctuations. This corresponds basically to the observations shown in Figures 2.3.a and 2.3.b. Inserting

$$\rho^a(x) = \rho^b(x) = \frac{1}{2},$$

in (4.23), and setting

$$g(x) = g^a(x) + ig^b(x), \quad W(x) = W^a(x) + iW^b(x), \quad (4.27)$$

we get solutions of the form

$$g(x) = -2i\eta \int_0^x e^{i\eta(u-x)} dW(u),$$

which corresponds to

$$q^a(x) = \frac{1}{2} + \frac{\eta}{\sqrt{N}} \left[\int_0^x (\sin(\eta(u-x)) dW^a(u) + \cos(\eta(u-x)) dW^b(u)) + dW^a(x) \right] + o\left(\frac{1}{\sqrt{N}}\right),$$

$$q^b(x) = \frac{1}{2} + \frac{\eta}{\sqrt{N}} \left[\int_0^x (\cos(\eta(u-x)) dW^a(u) - \sin(\eta(u-x)) dW^b(u)) + dW^b(x) \right] + o\left(\frac{1}{\sqrt{N}}\right).$$

Hence we have derived an *equivalent* process, which up to order $o\left(\frac{1}{\sqrt{N}}\right)$, describes the curves numerically observed. Letting

$$\begin{cases} h_N^a(x) \stackrel{\text{def}}{=} \frac{1}{N} \sum_{j=1}^{[xN]} (2s_j^a - 1), \\ h_N^b(x) \stackrel{\text{def}}{=} \frac{1}{N} \sum_{j=1}^{[xN]} (2s_j^b - 1), \end{cases}$$

the so-called equivalence says precisely

$$dh_N^a(x) = h_N^a\left(x + \frac{1}{N}\right) - h_N^a(x) = 2q_N^a(x) + \frac{2}{\sqrt{N}} \sigma_N^a(x) dW^a(x) - 1 + o\left(\frac{1}{\sqrt{N}}\right)$$

and the same holds for $dh_N^b(x)$. Introducing the complex function

$$h_N(x) = h_N^a(x) + ih_N^b(x),$$

we have

$$dh_N(x) = -\frac{2i\eta}{\sqrt{N}} \left[\int_0^x e^{i\eta(u-x)} dW(u) + dW(x) \right] + o\left(\frac{1}{\sqrt{N}}\right),$$

which, after integrating by parts, yields

$$h_N(x) = \frac{1}{\sqrt{N}} \left[\int_0^x 2e^{i\eta(u-x)} dW(u) - W(x) \right] + o\left(\frac{1}{\sqrt{N}}\right).$$

At this point it is possible to reconstruct the curves observed numerically, remembering that the discrete displacements (dx_i, dy_i) in the plane are expressed in terms of s_i^a and s_i^b as

$$\begin{cases} dx_i = 1 - s_i^a - s_i^b, \\ dy_i = s_i^a - s_i^b. \end{cases}$$

According to (4.27), we define

$$h(x) = \lim_{N \rightarrow \infty} \frac{1}{\sqrt{N}} \sum_{k=0}^{[xN]} (dx_k + idy_k) \quad \text{and} \quad Z(x) = \frac{i-1}{2} W(x).$$

Then we have

$$h(x) = \int_0^x 2 \exp[i\eta(u-x)] dZ(u) - Z(x).$$

This above equation accounts for the windings of the Brownian curve observed in figure 2.3.b. When $\eta \rightarrow 0$, $h(x)$ coincides with the standard Brownian motion Z .

4.4 Burgers equations in the fluid limit

In this section we give a formal derivation of dynamical equations describing the fluid limit, which includes the steady state solutions obtained in 4.3, without pretending to a rigorous presentation.

We start from the heuristic assumption that the conditional independence of the s_i^a [resp. s_i^b], which is realized at time $t = 0$ and at steady state, remains valid for all fixed time t , up to order $O(N^{-1})$. Exact proofs of this fact could be provided by adapting (up to sharp technicalities) some lines of argument proposed e.g. in [19, 10]), together with a mean field type approach for the convergence of the semi-groups of the underlying Markov processes indexed by N .

Considering the stochastic variable expressing the current of particles (a) between sites i and $i + 1$ at time t

$$\begin{aligned} \varphi_i^a(t) &= \lambda_a^+(i, t) s_i^a(t) \bar{s}_{i+1}^a(t) - \lambda_a^-(i, t) s_{i+1}^a(t) \bar{s}_i^a(t), \\ \varphi_i^b(t) &= \lambda_b^+(i, t) s_i^b(t) \bar{s}_{i+1}^b(t) - \lambda_b^-(i, t) s_{i+1}^b(t) \bar{s}_i^b(t), \end{aligned}$$

we define the conditional expectation

$$J_i^a(t) = \mathbb{E}[\varphi_i^a(t) \mid S^b], \quad J_i^b(t) = \mathbb{E}[\varphi_i^b(t) \mid S^a].$$

On account of the particle conservation principle, we have locally

$$\frac{\partial}{\partial t} \mathbb{E}[s_i^a(t)] + \mathbb{E}[\varphi_i^a(t) - \varphi_{i-1}^a(t)] = 0. \quad (4.28)$$

Then introducing the time dependent expectations $q_k^a(t)$ as functions of the sample path S^b

$$q_k^a(t) = \mathbb{E}[s_k^a(t) \mid S^b], \quad q_k^b(t) = \mathbb{E}[s_k^b(t) \mid S^a], \quad (4.29)$$

we can write by (4.28)

$$\frac{1}{N} \sum_{k=1}^N \alpha_k \left(q_k^a(t) - q_k^a(0) + \int_0^t d\tau (J_k^a(\tau) - J_{k-1}^a(\tau)) \right) = 0, \quad (4.30)$$

with again the condition $\sup_k |\alpha_k| < \infty$. Expressing the *almost* conditional independence of the s_k^a 's, we have

$$\begin{aligned} \frac{1}{N} \sum_{k=1}^N \alpha_k \mathbb{E}_t \left[\lambda_a^+(k, t) q_k^a(t) (1 - q_{k+1}^a(t)) - \lambda_a^-(k, t) q_{k+1}^a(t) (1 - q_k^a(t)) \right] = \\ \frac{1}{N} \sum_{k=1}^N \alpha_k J_k^a(t) + o\left(\frac{1}{N}\right). \end{aligned}$$

To be consistent with the procedure developed for the stationary regime case, we substitute to the S^b the so-called equivalent set $\{q_k^b + \sigma_k^b w_k^b\}$ into the expressions of the rates given by

$$\begin{aligned} \log \lambda_a^\pm(i) &= \log \lambda + 2(s_i^b + s_{i+1}^b - 2s_i^b s_{i+1}^b) \log \frac{\gamma}{\lambda} \\ &\pm \frac{\eta}{N} (1 - s_i^b - s_{i+1}^b) \pm \frac{\delta}{\gamma} (s_i^b - s_{i+1}^b) + o\left(\frac{1}{N}\right), \end{aligned}$$

according to the *fundamental scaling*. This insures that λ_a^+ and λ_a^- remain perfectly correlated. As for the the fluid limit, the procedure amounts simply to replace s_i^b by q_i^b in $\lambda_a^\pm(i)$, and to approximate all discrete sums in (4.30) by Riemann's integrals, for arbitrary $\alpha(x)$. This yields the continuity equation

$$\frac{\partial \rho^a(x, t)}{\partial t} = - \frac{\partial J^a(x, t)}{\partial x}, \quad (4.31)$$

where $\rho_a(x, t)$ and $J^a(x, t)$ are the deterministic continuous counterparts of $q_k^a(t)$ and $J_k^a(t)$. The current is now given by

$$J^a(x, t) = D \left[2\eta \rho^a (1 - \rho^a) (1 - 2\rho^b) - \frac{\partial \rho^a(x, t)}{\partial x} \right] \exp\left(2\rho^b (1 - \rho^b) \log \frac{\gamma}{\lambda}\right), \quad (4.32)$$

where we have introduced the diffusion constant

$$D \stackrel{\text{def}}{=} \lim_{N \rightarrow \infty} \frac{\lambda}{N^2},$$

λ being implicitly taken as a function of N . This scaling is confirmed numerically (see figure 2.6.c). Actually we observe that the parameter γ controls the dynamics of the system through the definition of an effective diffusion constant. For particles (a), we have

$$D^a(x, t) \stackrel{\text{def}}{=} D \exp\left[2\rho^b(x, t)(1 - \rho^b(x, t)) \log \frac{\gamma}{\lambda}\right].$$

with the corresponding relation for particles (b)). In the particular case $\gamma \rightarrow 0$, this constant vanishes, except at loci where the density of particles (b) has no fluctuations, that is $\sigma^2 = \rho^b(1 - \rho^b) = 0$, in which case $D^a(x, t) = D$, as to be expected from the analysis of the stretched walk. When $\gamma = \lambda$, we obtain a dynamical system of deterministic equations

$$\begin{aligned} \frac{\partial \rho^a(x, t)}{\partial t} &= D \frac{\partial^2 \rho^a(x, t)}{\partial x^2} - 2D\eta \frac{\partial}{\partial x} [\rho^a(1 - \rho^a)(1 - 2\rho^b)](x, t), \\ \frac{\partial \rho^b(x, t)}{\partial t} &= D \frac{\partial^2 \rho^b(x, t)}{\partial x^2} + 2D\eta \frac{\partial}{\partial x} [\rho^b(1 - \rho^b)(1 - 2\rho^a)](x, t). \end{aligned}$$

These equations belong to Burgers' class. When taking one of the two density species (say (a)) to be a constant $\rho_a = 0$ or $\rho_a = 1$, the density of particles (b) is driven by an ordinary Burgers equation, describing the evolution of a stretched walk. For an arbitrary γ , the steady state solution of (4.31) is tantamount to let the current vanish in (4.32), which after integration gives system (4.18) independent of γ , as to be expected.

5 Conclusion

The model of the discrete event system presented in this report turned out very friendly for simulation runs. Although the dimension be small (curves in the Euclidean plane), several basic phase-transition phenomena have been observed, among which a glassy phase. As we stoved to point out, there are many ways to describe this system, which bring to light connections between various stochastic and algebraic formalisms.

Nonetheless, in our opinion, the most efficient way toward concrete mathematical and physical properties appears to be on the track of coupled exclusion processes. This mapping allows also to address the continuous limit considered in the last section, and this approach can be a method for coding numerical simulations. In this manner, we have been able to observe that when we alternatively freeze one of the subsystems, letting the other one reach its equilibrium, the whole process attains its stationary state, and moreover much quicker.

With regard to the dynamic, deeper investigations are needed in order to include fluctuations directly into the equations, and to clarify the role of the parameter δ . This would give a firm starting point to get an insight into slow dynamics and into the non-linear excitations which are swarming in the glassy phase (metastable states). Open boundary conditions and presence of currents would also be worth investigating. Actually, it could be most rewarding (and this not hopeless) to generalize the model to higher dimensions and to find related concrete applications, for example in biology (evolution of RNA and proteins).

Acknowledgment The authors want to thank Arnaud de La Fortelle (INRIA) and Kirone Mallick (CEA) for many valuable discussions. The second author also acknowledges Christophe Josserand (CNRS) for useful advices, especially about numerical experiments.

References

- [1] P.G. De Gennes 1979 *Scaling Concepts in Polymer Physics* (Ithaca, NY: Cornell University Press).
- [2] M. Doi and S.F. Edwards 1986 *The Theory of Polymer dynamics* (Oxford University Press).
- [3] F. Spitzer, Trans. Am. Math. Soc. **87** (1958) 187
- [4] P. Lévy 1948 *Processus Stochastiques et Mouvement Brownien* (Gauthier-Villars).
- [5] J.W. Pitman, M. Yor, Ann. Probab. **17** (1989) 965
- [6] Ch.L. Berthelsen, J.A. Glazier, M.H. Skolnick, Phys. Rev. A **45** (1992) 8902–8913.
- [7] J.M. Burgers, Adv. Appl. Mech. **1** (1949) 177.
- [8] S. Cebrat, M. Dudek *The effect of DNA phase structure on DNA walks*. The Eur. J. Phys. **B 3** (1998) 271–276.
- [9] A. Comtet, J. Desbois, S. Ouvry, J. Phys. A: Math. Gen. **23** (1990) 5637.
- [10] R. Durrett (1995) *Ten lectures on particle systems*. Lecture Notes in Maths. 1608, Springer, 97–201.
- [11] P.E. Rouse, J. Chem. Phys. **21**, 1273. (1953)
- [12] O. Bénichoux, J. Desbois, J. Phys. A: Math. Gen. **33** (2000) 6655–6667.
- [13] V. Hakim, J.P. Nadal *Exact results for 2D directed animals on a strip of finite width*. J. Phys. A: Math. Gen. **16** (1983) L213.
- [14] J.S. Almeida, J.A. Carriço, A. Maretzek, P.A. Noble and M. Fletcher *Analysis of genomic sequences by Chaos Game Representation* J. of Bioinfo. **17** 5 (2001) 429–437.
- [15] J.R. Dorfman 1999 *An Introduction to Chaos in Nonequilibrium Statistical Mechanics*. Cambridge University Press.
- [16] O. Kallenberg (2001) *Foundations of Modern Probability*. Second Edition, Springer.
- [17] M. Kardar, G. Parisi and Y.C. Zhang, Phys. Rev. Lett. **56** (1986) 889.
- [18] J. Komlos, P. Major, G. Tusnady (1975,1976) *An approximation of partial sums of independent RV's and the sample DF I,II*. Z. Warsch. verw. Gebiete. **32**, 111–131.
- [19] T.M. Liggett (1985) *Interacting Particle Systems*. Grundlehren der mathematischen Wissenschaften, Springer.

- [20] B. Doubrovine, S. Novikov, A. Fomenko (1979) *Géométrie Contemporaine. 2e partie Géométrie et Topologie des Variétés*. Éditions Mir.
- [21] B. Derrida, M.R. Evans, V. Hakim and V. Pasquier *Exact solution for 1D asymmetric exclusion model using a matrix formulation* J. Phys. A: Math. Gen. **26** (1993) 1493–1517.
- [22] B.K. Øksendal (1985) *Stochastic Differential Equations*. Springer.